of new, chemically durable and radiation-tolerant hosts for safe and reliable storage of radioactive wastes and surplus actinides.

References and Notes

1. R. C. Ewing, W. Lutze, W. J. Weber, *J. Mater. Res.* **10**, 243 (1995).
2. R. C. Ewing, W. J. Weber, F. W. Clinard Jr., *Prog. Nucl. Energy* **29**, 63 (1995).
3. W. J. Weber, *Radiat. Eff.* **77**, 295 (1983).
4. F. W. Clinard Jr., D. L. Rohr, R. B. Roof, *Nucl. Instrum. Methods Phys. Res. B* **1**, 581 (1984).
5. F. W. Clinard Jr., G. F. Hurley, L. W. Hobbs, *J. Nucl. Mater.* **108/109**, 655 (1982).
6. L. W. Hobbs and F. W. Clinard Jr., *J. Phys. (Paris)* **41**, C6-232 (1980).
7. C. A. Parker, L. W. Hobbs, K. C. Russell, F. W. Clinard Jr., *J. Nucl. Mater.* **133/134**, 741 (1985).
8. K. E. Sickafus *et al.*, *J. Nucl. Mater.* **219**, 128 (1995).
9. Natural pyrochlore (ideally with the composition $NaCaNb_2O_6F$) contains U and Th in concentrations ranging from trace amounts to major proportions. Pyrochlore-bearing host rocks of age 10^6 to 10^9 years have experienced alpha-decay dose levels between 2×10^{14} and 3×10^{17} α/mg [G. R. Lumpkin, K. P. Hart, P. J. McGlinn, T. E. Payne, *Radiochim. Acta* **66/67**, 469 (1994)]. This self-radiation damage causes natural pyrochlore to undergo a crystalline-aperiodic (or amorphous) transformation with increasing dose.
10. (3+, 4+) cubic oxide pyrochlores contain eight molecules of $A_2B_2O_6O'$ (there are four nonequivalent atoms in the pyrochlore unit cell, hence the O′). The space group for the cubic pyrochlore structure is $Fd\bar{3}m$ [M. A. Subramanian, G. Aravamudan, G. V. Subba Rao, *Prog. Solid State Chem.* **15**, 55 (1983)]. Assuming the origin of the unit cell is centered on a B atom, each unit cell consists of 16 B cations at equipoint 16c (Wycoff notation), 16 A cations at equipoint 16d, 48 O anions at equipoint 48f, and 8 O′ anions at equipoint 8b.
11. M. Born, *Atomtheorie des Festen Zustandes* (Teubner, Leipzig, Germany, 1923).
12. M. O. Zacate, L. Minervini, D. J. Bradfield, R. W. Grimes, K. E. Sickafus, *Solid State Ionics*, **128**, 243 (2000).
13. M. Leslie, "DL/SCI/TM31T" *Technical Report* (UK Science and Engineering Research Council, Daresbury Laboratory, Warrington, UK, 1982).
14. Cation radii were obtained from R. D. Shannon [*Acta Crystallogr. A* **32**, 751 (1976)].
15. The absolute values of the cation antisite formation energies in Fig. 1 are too high to be compatible with the large degrees of disorder found in some pyrochlores. This problem was resolved by considering defect clusters that include both cation antisite and anion Frenkel pairs [L. Minervini, R. W. Grimes, K. E. Sickafus, *J. Am. Ceram. Soc.*, in press]. However, the qualitative picture presented by the results in Fig. 1 is unchanged.
16. We produced similar contour plots to the plot in Fig. 1 for other point defect reactions pertaining to a radiation damage environment. These included both cation and anion Frenkel defect reactions. In all cases, the qualitative features of the defect contour plots (*29*) are identical to Fig. 1; only the quantitative defect energies were found to vary from reaction to reaction. Results indicate that the highest defect energies belong to compounds with large A cations and comparatively smaller B cations, independent of the specific reaction. We contend that these point defect formation energies should correlate with lattice destabilization and ultimately, with amorphization. Lattice energies will rise with increasing defect concentrations more rapidly in compounds possessing high defect energies. In such materials, the free energy of the solid will overtake the free energy of an aperiodic structural phase, earlier than it will in materials with low defect energies. This makes compounds with high defect energies more susceptible to amorphization transformations.
17. E. M. Levin, C. R. Robbins, H. F. McCurdie, Eds., *Phase Diagrams for Ceramists* (American Ceramic Society, Columbus, OH, 1964–1999).
18. D. J. M. Bevan and E. Summerville, in *Handbook of the Physics and Chemistry of Rare Earths*, K. A. J. Gschneidner and L. Eyring, Eds. (Elsevier Science Publishers, Amsterdam, 1979), vol. 3, pp. 401–524.
19. A. W. Sleight, *Inorg. Chem.* **8**, 1807 (1969).
20. The anion lattice in pyrochlore compounds exhibits distortions compared to the diagram in Fig. 2. The oxygen ions on 48f lattice sites are displaced from the ideal positions indicated in Fig. 2, as described by the oxygen parameter, *x*. In an ideal pyrochlore, as shown in Fig. 2, $x = 0.375$.
21. The fluorite structure belongs to space group $Fm\bar{3}m$ [from JCPDS file 01-1274, International Committee for Diffraction Data, *Powder Diffraction File* (Joint Committee on Powder Diffraction Standards, Philadelphia, 1974 to present)]. Using the conventional setting for an MX_2 compound in this space group, cations reside at the origin and on a 4a equipoint, and anions are located on an 8c equipoint.
22. Cation Frenkel pairs will also form, but our calculations indicate that their formation energies are significantly higher than anion Frenkels and cation antisites (*29*). We observed the same trends in cation Frenkel formation energies (*29*) as for cation antisite defects (Fig. 1).
23. S. X. Wang, L. M. Wang, R. C. Ewing, G. S. Was, G. R. Lumpkin, *Nucl. Instrum. Methods Phys. Res. B* **148**, 704 (1999).
24. We grew single crystals of $Er_2Ti_2O_7$ and $Er_2Zr_2O_7$ in a Crystal Systems, Inc. floating-zone crystal growth unit. X-ray diffraction (XRD) measurements on powders obtained from the crystal boules indicated that both the $Er_2Ti_2O_7$ and $Er_2Zr_2O_7$ are cubic, with lattice parameters given by $a = 1.0095(1)$ nm for $Er_2Ti_2O_7$ and $a = 0.5198(1)$ nm for $Er_2Zr_2O_7$ (using a silicon internal standard). Our XRD results are consistent with a pyrochlore structure for the $Er_2Ti_2O_7$ crystal and a fluorite structure for the $Er_2Zr_2O_7$ crystal.
25. S. X. Wang *et al.*, *J. Mater. Res.* **14**, 4470 (1999).
26. H. Matzke and M. Kinoshita, *J. Nucl. Mater.* **247**, 108 (1997).
27. K. E. Sickafus *et al.*, *J. Nucl. Mater.* **274**, 66 (1999).
28. The factors controlling void swelling are not always related to those controlling amorphization. Additional experiments are needed to determine comparative void swelling rates in pyrochlore and fluorite compounds. Nevertheless, because of the complex chemistry and structure characteristics of these $A_2B_2O_7$ compounds, we anticipate minimal swelling behavior for this class of oxides.
29. L. Minervini, R. W. Grimes, K. E. Sickafus, data not shown.

30. Sponsored by the U.S. Department of Energy, Office of Basic Energy Sciences, Division of Materials Sciences.

28 March 2000; accepted 8 June 2000

Aggregation-Based Crystal Growth and Microstructure Development in Natural Iron Oxyhydroxide Biomineralization Products

Jillian F. Banfield,[1]* Susan A. Welch,[1] Hengzhong Zhang,[1] Tamara Thomsen Ebert,[2] R. Lee Penn[3]

Crystals are generally considered to grow by attachment of ions to inorganic surfaces or organic templates. High-resolution transmission electron microscopy of biomineralization products of iron-oxidizing bacteria revealed an alternative coarsening mechanism in which adjacent 2- to 3-nanometer particles aggregate and rotate so their structures adopt parallel orientations in three dimensions. Crystal growth is accomplished by eliminating water molecules at interfaces and forming iron-oxygen bonds. Self-assembly occurs at multiple sites, leading to a coarser, polycrystalline material. Point defects (from surface-adsorbed impurities), dislocations, and slabs of structurally distinct material are created as a consequence of this growth mechanism and can dramatically impact subsequent reactivity.

In natural systems, growth of crystals has typically been thought to occur by atom-by-atom addition to an inorganic or organic template or by dissolution of unstable phases (small particles or metastable polymorphs) and reprecipitation of the more stable phase. However, a growing body of experimental work indicates that additional self-assembly–based coarsening mechanisms can operate in certain nanophase materials under some conditions (*1–7*). Here, we show that iron oxyhydroxide crystals can grow via an aggregation-based pathway under natural conditions and discuss the ways in which this mechanism can control the form and reactivity of nanophase materials in nature.

Microorganisms catalyze iron oxidation in acidic and near-neutral solutions, leading to accumulations of iron oxyhydroxides. This process may have been important in formation of Proterozoic banded iron formations (*8*). Nanophase iron oxyhydroxides can also

[1]Department of Geology and Geophysics, University of Wisconsin–Madison, Madison, WI 53706, USA. [2]Diversions Scuba, Madison, WI 53705, USA. [3]Department of Earth and Planetary Sciences, Johns Hopkins University, Baltimore, MD 21218, USA.

*To whom correspondence should be addressed. E-mail: jill@geology.wisc.edu

form abiogenically (e.g., due to neutralization of acidic iron-rich solutions and as the result of chemical weathering of iron-rich minerals). Iron oxyhydroxides (and aluminum oxyhydroxides, which share similar crystal chemical characteristics) are common in surficial materials and may compose the bulk of their reactive surface area.

We examined samples from the flooded, carbonate-hosted Piquette Pb-Zn mine beneath Tennyson, Wisconsin (water pH, ~8). Iron-oxidizing microorganisms congregate in redox transition zones within the water column in the tunnels. In the ~30 years since the mine flooded, tens of centimeter-thick orange stalactites and stalagmites and slime layers have accumulated (Fig. 1).

Samples of the water and slime were collected by a SCUBA diving team (*9*). Optical and transmission electron microscopic (TEM) examination of the slime (with a 200-kV TEM) revealed that it consists of colloidal aggregates of nanoparticles, mineralized cell products, and cells (Fig. 2). The twisted stalks are characteristic of iron-oxidizing bacteria belonging to the *Gallionella* genus. Sheathed elongate cells are typical of bacteria belonging to the iron-oxidizing *Lepthothrix* genus (*10*).

Colloids and coatings on organic cell, stalk, and sheath materials consist of ~2- to 3-nm diameter Fe-rich particles (Fig. 3). Selected area electron diffraction (SAED) patterns typically showed rings with diffuse intensity at ~0.25 and 0.15 nm, indicating the sample consists mostly of randomly oriented two-line ferrihydrite (*11–14*) (Fig. 3). In regions ranging from a few nanometers to hundreds of nanometers, however, the primary nanoparticles were not randomly oriented, but were ordered into clusters and chains (Fig. 4). This was most pronounced at the peripheries of mineralized organic material (stalks and sheaths) and in colloidal aggregates. Low contrast between crystalline (lattice-fringe–bearing) regions in higher resolution images indicated that space separated adjacent particles (Fig. 5). However, the parallelism of lattice fringes demonstrates that the crystallographic axes of all particles in this area are parallel. We interpret these regions as consisting of aggregates of particles that share the same three-dimensional (3D) orientation (a defective single crystal).

We suggest that these crystals formed as follows. It is well established that bacteria such as the *Gallionella* spp. and the *Leptothrix* spp. enzymatically oxidize dissolved ferrous iron. Due to the low solubility of ferric iron compounds at near-neutral pH, immediate solution supersaturation with respect to ferrihydrite solubility occurred. Most of the ~2- to 3-nm diameter particles formed in solution and either attached to surrounding negatively charged polymers (e.g., *Gallionella* stalks) or flocculated to form colloidal aggregates. The double layers separating surfaces of adjacent particles may have been eliminated after repulsive interactions were overcome as the result of random, Brownian motion–driven particle collisions. These collisions may have been especially effective because the double layer of each particle contained very little net charge because the pH was close to the average isoelectric point of iron oxyhydroxide crystal surfaces. Jiggling of nanoparticles by Brownian motion may also allow adjacent particles to rotate to find the low-energy configuration represented by a coherent particle-particle interface. Rotation of particles within aggregates may also be driven by short-range interactions between adjacent surfaces (*15*). In aggregation-based growth, reduction in surface free energy is achieved by complete removal of pairs of surfaces.

TEM data showed oriented aggregates within spatially confined regions separated from other adjacent regions of oriented particles by areas that were dominated by particles in random orientations. This suggests that oriented aggregation was initiated at multiple sites within colloids. The orientation adopted within one region was unrelated to that in an adjacent region. Therefore, we predict that coarsening will lead to a polycrystalline material composed of larger particles. Oriented aggregation was most commonly detected in colloids and in particle aggregates at the peripheries of bacterial stalks and sheaths. We attribute the less extensive coarsening of ferrihydrite bound to stalks and cell sheaths to the inhibition of crys-

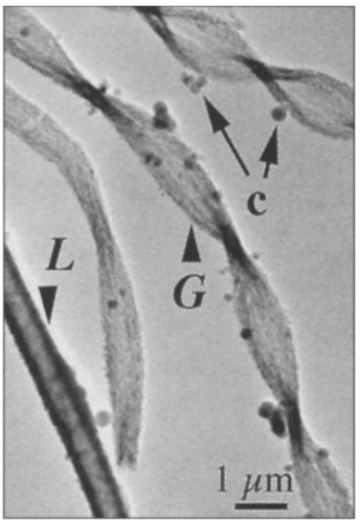

Fig. 2. TEM image of *Gallionella* stalks (G) and a *Leptothrix* sheath (L). Contrast associated with the stalks and sheath is due to nanoparticulate iron oxyhydroxides. Colloidal aggregates of nanoparticles (c) are also present.

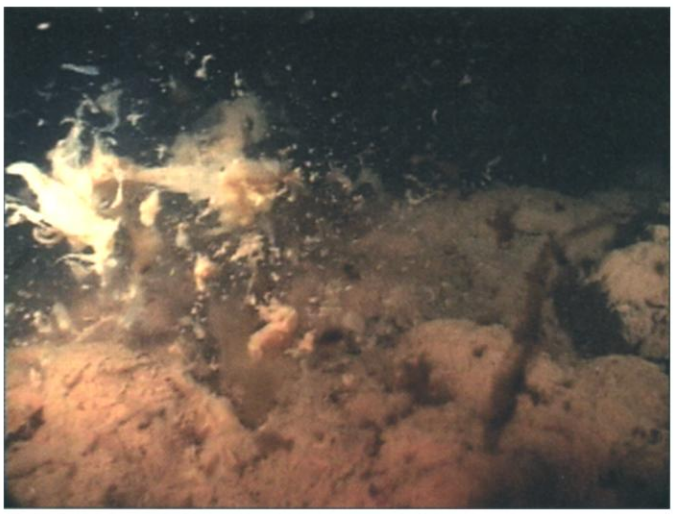

Fig. 1. Photograph taken underwater in the Piquette mine showing accumulations of orange, polymer-laden ferric iron oxyhydroxides. Tens of centimeter-wide clumps of suspended material were displaced by passage of the leading diver. Image courtesy of T. O'Connor.

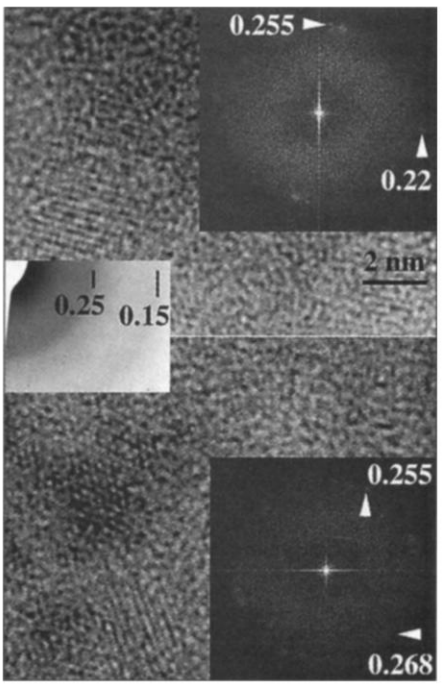

Fig. 3. HRTEM images of ~ 2 to 3 nm diameter iron oxyhydroxide particles. Insets are Fourier transforms (FT) of image regions showing diagnostic interplanar spacings (in nanometers), and selected area electron diffraction pattern (left) is typical of two-line ferrihydrite.

tal rotation by interactions between the particles and the polymer substrate. It is possible that the distinctive stalk or cell morphologies (potential biosignatures) will be preserved by textural differences, including smaller particle size compared to surrounding materials.

Crystal growth by oriented attachment has important implications for subsequent materials reactivity. Phase stability can be particle size–dependent, so crystal growth can promote phase transformation (*16–19*). Phase transformation is also induced if initial precipitates are metastable. In our samples, laths of goethite (FeOOH) (Fig. 6A) are intergrown within regions of coarsened ferrihydrite. Observed crystal orientations (Fig. 6B) ensure the maximum continuity between the closest packed oxygen planes of goethite and ferrihydrite, which is presumed to be the goethite precursor. Goethite can form from ferrihydrite largely by relocation of a subset of iron atoms into adjacent face-sharing octahedral sites and small displacements of every fourth oxygen plane.

Surfaces of nanocrystalline iron oxyhydroxides in the environment are active adsorption sites (e.g., for arsenate or phosphate in acidic solutions and metals in alkaline solutions). If aggregation-based growth occurs, adsorbed ions at particle surfaces may be incorporated as point defects. This could decrease the bioavailability of these ions and could modify the thermodynamic properties and kinetic behavior of the material.

Previous experimental studies have shown that line defects (*3*) are introduced when growth occurs by oriented aggregation. Dislocations form at interfaces when surfaces of adjacent oriented particles are not atomically flat. Such dislocations are common at low-angle grain boundaries in arrays of ferrihydrite particles and are present in goethite (Fig. 6A). These defects can fundamentally impact subsequent coarsening (e.g., by spiral growth) and deformation.

Oriented attachment requires coherence in the two-dimensional (2D) plane of the interface. This can be achieved in a way that ensures perfect structural continuity across the interface, or new 3D structural units can be created (*4, 5*). These units may be characteristic of a more stable phase and provide nuclei for the phase transformation. Thus, planar defects introduced during growth by oriented attachment can increase rates of subsequent reactions by lowering the activation barrier. In the case of ferrihydrite, incomplete double chains of Fe octahedra, similar to the double chains found parallel to [001] goethite, can be created at coherent interfaces (*20*). Schwertmann *et al.* (*21*) showed that recrystallization and transformation were enhanced by particle aggregation. Our results provide an atomistic explanation for these phenomena.

Aggregation may occur at finer scales than reported here. Assembly of multinuclear clusters (*22*) may be a very early crystallization step. Periodic, few-octahedra–wide vacancies characteristic of (six-line) ferrihydrite (*14*) are explained if ferrihydrite is constructed from subnanometer-scale clusters, which are also formed by aggregation of aqueous ions (*23*). Thus, crystals may grow by assembly of increasingly large units in a process analogous to the formation of hundred-nanometer–wide particles from few-nanometer-diameter particles (as in Fig. 5). This pathway may dominate over dissolution-recrystallization if the phase is relatively insoluble.

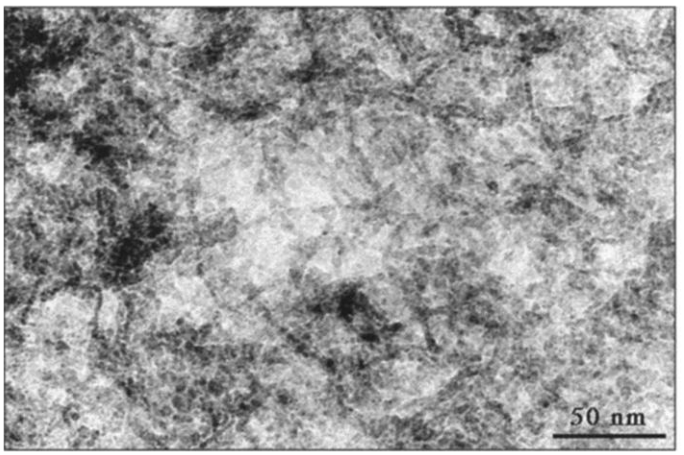

Fig. 4. TEM image of an area within a colloidal aggregate of ferrihydrite nanocrystals. Chains and aggregates indicate self-assembly of particles.

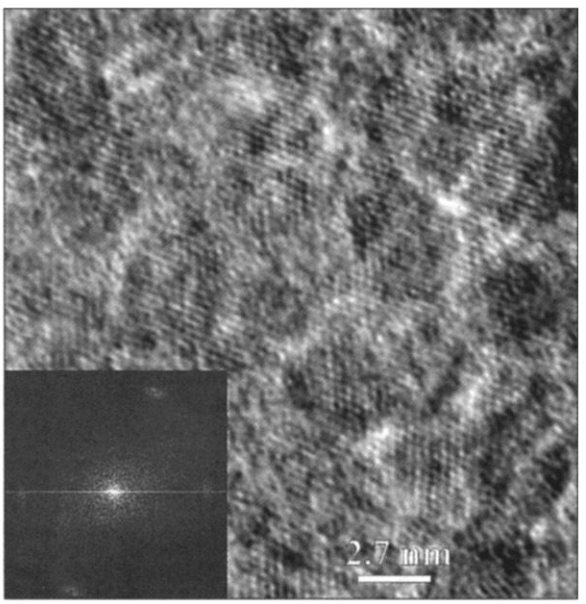

Fig. 5. HRTEM image of an aggregate of ferrihydrite nanocrystals. Low contrast between crystalline regions (lattice fringes) indicates that space separates most particles. Lattice fringe orientations and FT (inset) demonstrate that particles have been assembled so they share a single crystallographic orientation (see Web fig. 1, A through F, for more examples) (*24*).

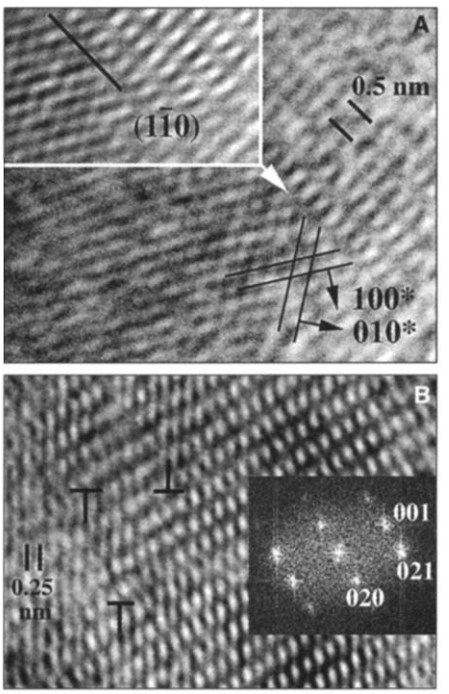

Fig. 6. (**A**) HRTEM image of goethite containing three edge dislocations interpreted to have formed due to imperfectly oriented aggregation (see Web fig. 2, A and B, for more examples) (*24*). (**B**) HRTEM image showing the ferrihydrite-goethite interface, reactant, and product orientations. These are consistent with growth of goethite directly from ferrihydrite (see Web fig. 3) (*24*).

References and Notes

1. A number of experimental studies describe growth via oriented aggregation. For example, this has been reported in anatase (TiO_2) under hydrothermal conditions [R. L. Penn and J. F. Banfield, *Geochim. Cosmochim. Acta* **63**, 1549 (1999)]. Also see (*2–7*).
2. Aggregation-based grown has been demonstrated in hematite (α-Fe_2O_3) formed by aging of $FeCl_3$ in the presence of KH_2PO_4 [J. K. Bailey, C. J. Brinker, M. L Mecartney, *J Colloid. Interface Sci.* **157**, 1 (1993)].
3. R. L. Penn and J. F. Banfield, *Science* **281**, 969 (1998).
4. _____, *Am. Mineral.* **83**, 1077 (1998).
5. _____, *Am. Mineral.* **84**, 871 (1999).
6. K. Onuma and A. Ito, *Chem. Mater.* **10**, 3346 (1998).
7. V. Privman, D. V. Goia, J. Park, E. J. Matijevic, *J. Colloid. Interface Sci.* **213**, 36 (1999).
8. D. Emerson and C. Moyer, *Appl. Environ. Microbiol.* **63**, 4784 (1997).
9. A mine-trained SCUBA diving team led by T. T. Ebert collected samples of water and biofilms into sterile syringes. Samples were kept on ice until returned to the laboratory, where they were stored at 4°C before examination by optical and electron microscopy.
10. Cells were detected by staining their DNA with 4′,6-diamidino-2-phenylindole (DAPI). Stained cells were visualized with epifluorescence microscopy. Population analyses with 16*S* ribosomal RNA gene sequencing are underway. Results will be reported separately.
11. High-resolution TEM (HRTEM) images show cross-fringes (periodicities not detected by SAED) in orientations that indicate 3D order in two-line ferrihydrite (see Fig. 3). In some regions, additional diffraction maxima indicate feroxyhite (*12*) and, less commonly, six-line ferrihydrite. Results are consistent with previous studies (*13*, *14*), which provide structural details.
12. V. A. Drits, B. A Sakharov, A. Manceau, *Clay Miner.* **28**, 209 (1993).
13. A. Manceau and V. A. Drits, *Clay Miner.* **28**, 165 (1993).
14. V. A. Drits, B. A Sakharov, A. L. Salyn, A. Manceau, *Clay Miner.* **28**, 185 (1993).
15. H. L. Zhu and R. S. Averback [*Philos. Mag.* **73**, 27 (1996)] demonstrated rotation of copper particles to achieve parallel orientations with molecular dynamics simulation. The homogeneous sizes of the initial nanoparticles and their clear separation into distinct 2- to 3-nm diameter entities rule out an alternative interpretation that oriented aggregates arise from sequential nucleation of seeds on earlier formed particles. No damage (such as creation of porosity) was detected during examination with the HRTEM operated at 200 kV. No microstructures suggestive of contact epitaxy were observed.
16. D. Langmuir, *Am. J. Sci.* **271**, 147 (1971).
17. A. A. Gribb and J. F. Banfield, *Am. Mineral.* **82**, 717 (1997).
18. J. M. McHale, A. Auroux, A. J. Perrotta, A. Navrotsky, *Science* **277**, 788 (1997).
19. H. Zhang and J.F. Banfield, *J. Mater. Chem.* **8**, 2073 (1998).
20. Oriented aggregation requires coherency in the 2D plane of the interface. In addition to attachment that generates perfect 3D structure, coherent {100} and {110} interfaces with structural characteristics intermediate between ferrihydrite and goethite can be created. These regions may nucleate transformation reactions. We reported analogous phenomena in titania; see (*4*, *5*).
21. U. Schwertmann, J. Friedl, H. J. Stanjek, *J. Colloid Interface Sci.* **209**, 215 (1999).
22. For example, see O. Y. Pykhteev, A. A. Efimov, L. N. Moskvin, *Russ. J. Appl. Chem.* **72**, 9 (1999). Although some data supporting the formation of polynuclear hydrolysis products have been reported, Schwertmann *et al.* (*21*) maintain that there is no good evidence for intermediates between trimers and solids.
23. Subnanometer-scale porosity within ferrihydrite (*7*) may be generated if ferrihydrite itself forms by aggregation of protocrystals. Protocrystals could consist of three oxygen planes that sandwich pairs of face-sharing octahedra (to our knowledge, no small aqueous clusters containing face-sharing units are known, so face-sharing must be introduced by aggregation of smaller corner- and edge-linked molecules). Formation of ferrihydrite could proceed via sequential elimination of n(OH), following aggregation of pairs of {~n[$O_{0.25}$ $(OH)_{0.75}$ $(Fe_{2/3})$ $O_{0.5}(OH)_{0.5}(Fe_{2/3})$ $O_{0.25}$ $(OH_{0.75})$or n$(FeOOH)_4 \cdot H_2O$] units}. If some factor favors joining of alternate nuclei that are rotated by 180°, ferrihydrite ABAC oxygen closest packing would result.
24. Web figures 1 through 3 are available at *Science* Online at www.sciencemag.org/feature/data/1050910.shl.

25. We thank V. Dritts and A. Manceau for their comments on a longer report describing structural aspects of iron oxyhydroxides and W. H. Casey for discussion of multinuclear clusters. Supported by NSF grants EAR 9317082 and EAR 9814333 and the NASA Astrobiology Institute (JPL-Caltech). We also thank T. O'Connor for permission to reproduce Fig. 1.

30 March 2000; accepted 19 June 2000

A Cyclic Carbanionic Valence Isomer of a Carbocation: Diphosphino Analogs of Diaminocarbocations

Tsuyoshi Kato,[1] Heinz Gornitzka,[1] Antoine Baceiredo,[1] Wolfgang W. Schoeller,[2] Guy Bertrand[1]*

Diaminocarbocations (or amidinium salts) feature a three-center 4π electron system with an open planar structure. Their 2π electron three-membered cyclic valence isomers, in which the carbon atom bears a negative charge, are predicted to be about 541 kilojoules per mole higher in energy than the open form. This isomer has not been identified yet. In contrast, the attempted synthesis of a diphosphorus analog of amidinium salts leads to the cyclic carbanionic form. There is no precedent for such a transformation of a carbocationic center into a carbanionic center, but with the help of heavier main-group elements, numerous examples can be imagined. This approach will enable the preparation of many unknown structural moieties that are difficult or even impossible to access in the corresponding carbon and nitrogen series.

In 1972, Olah suggested that cations of carbon compounds be termed "carbocations" (*1*); the corresponding anionic compounds are called "carbanions." Because they are not tetravalent, carbocations are usually very reactive, and in his Nobel lecture, Olah added, "it should be clear that in carbocationic systems varying degrees of delocalization always exist. This can involve participation by neighboring n-donor atoms, π-donor groups, or σ-donor C–H or C–C bonds" (*2*, p. 1401). The long-known synthetically and biologically important amidinium salts, $\mathbf{I_N}$, can thus be considered as diamino-substituted carbocations (*3–9*). Here, we report the synthesis of a diphosphorus analog, which adopts a cyclic structure $\mathbf{II_P}$, with the carbon atom bearing a negative charge (Fig. 1).

Quantum chemical calculations at the B3LYP/6-31g* level with additional zero-point vibrational energy correction (*10*) predict the amidinium salt $\mathbf{I_N}$ (R = R′ = H) to be 541 kJ/mol more stable than its unknown cyclic valence isomer $\mathbf{II_N}$. Several factors indicated that the difference in energy between the valence isomers $\mathbf{I_P}$ and $\mathbf{II_P}$ should be much smaller than in the nitrogen series. (i) A stable allylic structure of type **I** (a three-center 4π electron system) implies a large singlet-triplet energy separation, which amounts to 379 kJ/mol for the parent compound $\mathbf{I_N}$ but only 163 kJ/mol for $\mathbf{I_P}$ (R = R′ = H). This is due mainly to the much smaller inversion barrier at nitrogen (21 kJ/mol) than at phosphorus (146 kJ/mol), which favors π bonding. In addition, π bonds between phosphorus and carbon are much weaker than those for nitrogen (P=C, 188 kJ/mol; N=C, 271 kJ/mol), which disfavors the allylic structure $\mathbf{I_P}$. (ii) Phosphorus-carbon bonds are longer than

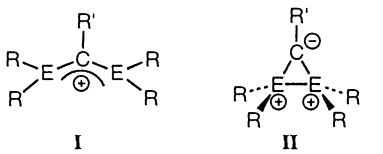

I **II**

$\mathbf{I_N}, \mathbf{II_N}$: E = N

$\mathbf{I_P}, \mathbf{II_P}$: E = P

Fig. 1. Diamino- and diphosphino-substituted carbocations **I** and their cyclic valence isomers **II**.

[1]Laboratoire d'Hétérochimie Fondamentale et Appliquée, Université Paul Sabatier, 118, route de Narbonne, F-31062 Toulouse cedex 04, France. [2]Fakultät für Chemie der Universität, Postfach 10 01 31, D-33615 Bielefeld, Germany.

*To whom correspondence should be addressed. E-mail: gbertran@ramses.ups-tlse.fr